Long wavelength bulk GaInNAs *p–i–n* photodiodes lattice matched to GaAs

J. S. Ng,[a] W. M. Soong, M. J. Steer, M. Hopkinson, and J. P. R. David
Department of Electronic and Electrical Engineering, University of Sheffield, Mappin Building, Mappin Street, Sheffield S1 3JD, United Kingdom

J. Chamings, S. J. Sweeney, and A. R. Adams
Advanced Technology Institute, School of Electronics and Physical Sciences, University of Surrey, Guildford, Surrey GU2 7XH, United Kingdom

(Received 31 August 2006; accepted 8 January 2007; published online 20 March 2007)

We report bulk GaInNAs *p–i–n* photodiodes lattice-matched to GaAs substrates, grown by solid source molecular beam epitaxy with photoresponses out to ~1.3 μm. The as-grown samples were characterized optically, structurally, and electrically. A low background doping concentration in the range of 10^{14}–10^{15} cm^{-3} was obtained in the samples. One of the samples with a 0.5 μm thick GaInNAs absorbing layer gave a responsivity of 0.11 A/W for a band edge of 1.28 μm at reverse bias of 2 V. © *2007 American Institute of Physics*. [DOI: 10.1063/1.2709622]

I. INTRODUCTION

The material $Ga_{1-x}In_xN_yAs_{1-y}$ has been attracting considerable interest recently because it can be grown lattice matched on GaAs substrates and has a narrower band gap than GaAs.[1] It can therefore extend the photoresponse of GaAs-based optoelectronic devices to beyond 1.3 μm, which previously could only be achieved by strained $In_xGa_{1-x}As$/GaAs quantum wells or metamorphic InGaAs layers.[2] Hence, there is interest in using this material for GaAs-based photodetectors[3–8] and multijunction photovoltaic cells.[9,10] GaAs-based photodetectors can utilize high-reflectivity AlAs/GaAs mirrors[4] and the $Ga_{1-x}In_xN_yAs_{1-y}$ material has been predicted to have low avalanche noise,[8] while photovoltaic cells can benefit from long wavelength absorption.

$Ga_{1-x}In_xN_yAs_{1-y}$ as grown for photodetectors and photovoltaic cells is distinct from the strained $Ga_{1-x}In_xN_yAs_{1-y}$ multiple quantum wells employed in 1.3 and 1.5 μm wavelengths laser diodes. For these former applications, high quality growth of thick (relative to quantum well dimensions) $Ga_{1-x}In_xN_yAs_{1-y}$ with good lattice matching to GaAs substrates and low unintentional doping concentration are essential. The thickness is required to ensure efficient absorption of incident light and hence high responsivity (for photodetectors) or efficiency (for photovoltaic cells). Any appreciable lattice mismatch to GaAs could therefore result in dislocations occurring which would adversely affect the device performance. The low unintentional doping concentration in the $Ga_{1-x}In_xN_yAs_{1-y}$ layer ensures full depletion, even at low reverse voltage, enabling low operating voltage photodetectors and high efficiency photovoltaic cells.

In order to operate at longer wavelengths, the band gap of $Ga_{1-x}In_xN_yAs_{1-y}$ has to decrease, which can be achieved by increasing the indium and the nitrogen content. However, the difficulty of incorporating significant amounts of nitrogen into $Ga_{1-x}In_xN_yAs_{1-y}$ is usually overcome by using a low growth temperature,[11–13] which can adversely affect the crystal quality. Therefore, an increasing nitrogen content is often linked to degradation in the optical and electrical properties of $Ga_{1-x}In_xN_yAs_{1-y}$ as indicated by reduced photoluminescence intensity[14,15] and a reduced open-circuit voltage for photovoltaic cells.[10] Postgrowth thermal annealing can sometimes improve the photoluminescence intensity[15] but this has the undesirable effect of increasing the $Ga_{1-x}In_xN_yAs_{1-y}$ band gap. To avoid over-reliance on postgrowth annealing to improve material quality, high quality, as-grown, thick $Ga_{1-x}In_xN_yAs_{1-y}$ layers with narrow band gap and lattice match to GaAs are required.

There have been several reports of photoluminescence and x-ray data obtained from thick $Ga_{1-x}In_xN_yAs_{1-y}$ (Refs. 10–14) but few reports on bulk $Ga_{1-x}In_xN_yAs_{1-y}$ device characteristics. Reports on the electrical characteristics and photoresponse of bulk $Ga_{1-x}In_xN_yAs_{1-y}$ diodes operating at wavelengths up to 1.3 μm are limited to.[4–7] The *p–i–n* diodes reported in Ref. 6 had $Ga_{1-x}In_xN_yAs_{1-y}$ *i* regions up to 2 μm thick, but the absorption edge was less than ~1.22 μm and the reverse dark currents were measured for a limited field range up to 25 kV/cm. Cheah *et al.*[5] compared the dark current characteristics of $Ga_{1-x}In_xN_yAs_{1-y}Sb$ and $Ga_{1-x}In_xN_yAs_{1-y}$ *p–i–n* diodes with an absorption edge at ~1.35 μm. They concluded that in order to simultaneously achieve a reasonably low reverse dark current and light absorption at ~1.3 μm, use of a pentanary bulk $Ga_{1-x}In_xN_yAs_{1-y}Sb$ *i* region was necessary. Ptak *et al.* reported unintentional doping concentration of 2×10^{13} cm^{-3} yielding a depletion width of 3 μm for $Ga_{1-x}In_xN_yAs_{1-y}$ diodes but the nitrogen content was relatively small, giving band gaps ranging from 1.26 to 1.34 eV.[9] Recently, Loke *et al.*[7] reported an as-grown $Ga_{1-x}In_xN_yAs_{1-y}$ *p–i–n* diode with 0.5 μm thick *i* region but the responsivity is rather low (0.016 A/W for a photon energy of 0.92 eV) and the reserve dark currents are very high.

In this article, we present our study on the optical, structural and electrical properties of a series of bulk

[a]Electronic mail: j.s.ng@sheffield.ac.uk

TABLE I. Structure details of the bulk $Ga_{1-x}In_xN_yAs_{1-y}$ $p-i-n$ mesa diodes used.

Layer	Nominal layer thickness: Wafer A (nm)	Nominal layer thickness: Wafers B and C (nm)
p^+ GaAs	1000	500
p^+ GaInNAs	200	50
i-GaInNAs	1000	400
n^+ GaInNAs	200	50
n^+ GaAs	1000	300
n^+ AlAs	100	100
n^+ GaAs	200	200
n^+ GaAs susbstrate		

$Ga_{1-x}In_xN_yAs_{1-y}$ $p-i-n$ diode wafers lattice matched to GaAs. We carried out measurements of x-ray rocking curves and photoluminescence on as-grown wafers as well as of capacitance-voltage, current-voltage, electroluminescence, and photocurrent on devices fabricated from the wafers.

II. WAFER STRUCTURES AND GROWTH

The series of wafers consist of three nominally lattice-matched $Ga_{1-x}In_xN_yAs_{1-y}$ $p-i-n$ diode wafers grown on (001) n^+ GaAs substrates using a VG Semicon V80H molecular beam epitaxy system equipped with conventional solid sources for group-III, Be for p type and Si for n type dopants, an Applied EPI cracker source for As_2, and an Oxford Applied Research radio frequency plasma source for the nitrogen. Structures of the three wafers studied are described in Table I. The doping concentrations in the GaAs and $Ga_{1-x}In_xN_yAs_{1-y}$ claddings were nominally 2×10^{18} cm^{-3}.

The n^+ and p^+ GaAs claddings were grown at 590 °C with a growth rate of 0.5 μm per hour. For the growth of the $Ga_{1-x}In_xN_yAs_{1-y}$ layer (including the p^+ and n^+ $Ga_{1-x}In_xN_yAs_{1-y}$ claddings) the temperature was reduced to 450 °C to encourage incorporation of nitrogen into the lattice-matched $Ga_{1-x}In_xN_yAs_{1-y}$ layer.[13] The growth rate for $Ga_{1-x}In_xN_yAs_{1-y}$ was 0.56 μm per hour. The nitrogen plasma source was operated with a radio frequency (rf) power of 184 W. Growth interruption was introduced between the growth of the n^+ GaAs cladding and the n^+ $Ga_{1-x}In_xN_yAs_{1-y}$ cladding in order to stabilize the rf power of the nitrogen plasma source. The characterization data reported later were obtained from as grown materials without postgrowth annealing. However some *in situ* annealing may have occurred during the growth of the p^+ GaAs cladding, which was maintained at 590 °C.

Some of the measurements carried out in this work had to be performed on fabricated devices. Circular mesa diodes with diameters of 400, 200, 100 and 50 μm were fabricated using standard photolithography and wet chemical etching. Top annular p-type Ohmic contacts (Au-Zn-Au) were deposited to allow optical access and n-type Ohmic contact (In-Ge-Au) was deposited onto the back of the substrates. To avoid unintentional postgrowth annealing, the metal contacts were annealed at ~360 °C, which is well below the growth temperature of $Ga_{1-x}In_xN_yAs_{1-y}$ used in this work.

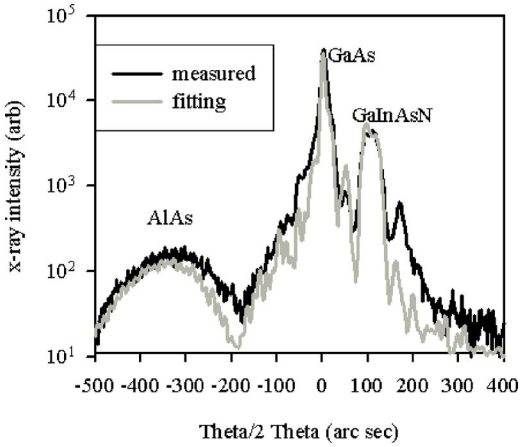

FIG. 1. Measured (black line) and fitted (gray line) x-ray rocking curve for the center of wafer C.

III. X-RAY ROCKING CURVES AND PHOTOLUMINESCENCE

X-ray double crystal rocking curves (theta/2 theta scans) diffracted off the (004) plane were measured on the as-grown wafers. The thin AlAs layer, a material usually considered lattice matched to GaAs, in the structures consistently gave a broad peak with peak splitting of ~−330 arc sec, which is expected from the AlAs layer thickness and the lattice constant, for all three wafers. The peak splitting values between the $Ga_{1-x}In_xN_yAs_{1-y}$ peak and the GaAs substrate peak measured near the center of wafers A, B, and C were found to be +136, +74, and +108 arc sec (tensile strain), corresponding to lattice mismatch (or strain) of -5.3×10^{-4}, -2.9×10^{-4}, and -4.2×10^{-4}, respectively. These values, summarized in Table II, are small compared to the −540 arc sec peak splitting in Ref. 6 and the lattice mismatch of 0.26% in Ref. 5. From critical layer thickness estimates,[16] we believe there is no significant relaxation in our samples.

An x-ray rocking curve near the center of wafer C is shown in Fig. 1. Analysis of the x-ray peak splitting[17] (assuming negligible relaxation in the $Ga_{1-x}In_xN_yAs_{1-y}$ layers) was carried out to deduce the nitrogen content. The indium contents for the $Ga_{1-x}In_xN_yAs_{1-y}$ layers in the three wafers were given by wafer growth calibration (x-ray rocking curve analyses of strained $In_xGa_{1-x}As/GaAs$ quantum wells wa-

TABLE II. Summary of bulk $Ga_{1-x}In_xN_yAs_{1-y}$ $p-i-n$ mesa diodes used in this work.

Wafer	Indium content (%)	Nitrogen content (%)	Electroluminescence peak (eV)	Peak splitting (arc sec)
A	3	1.4	1.28	+136
B	8	3.0	1.04	+74
C	10	3.8	0.97	+108

fers). Vegard's law was then used to linearly interpolate the $Ga_{1-x}In_xN_yAs_{1-y}$ layer lattice constant, a, from the lattice constants of the four binaries, a_{GaAs}, a_{InAs}, a_{InN}, and a_{GaN} to give value for x.

Using a nitrogen content of 3.8%, fitting to the measured x-ray rocking curve of wafer C is in agreement with the experimental data, as shown in Fig. 1. Similar interpretations of the x-ray rocking curves obtained near the centers of wafers A and B yielded nitrogen contents of 1.4% and 3.0%, respectively. These nitrogen contents are also summarized in Table II.

The linewidth of the x-ray peak of the $Ga_{1-x}In_xN_yAs_{1-y}$ layer provides a qualitative indication of crystal quality. The peaks due to the $Ga_{1-x}In_xN_yAs_{1-y}$ and the GaAs have linewidths of 41 and 13 arc sec (compared to 9 arc sec from simulations for a GaAs substrate), respectively, for wafer C, where nitrogen content of 3.8% was achieved. This compares favorably to the ~55 arc sec for a much lower nitrogen content of 0.55% reported in Ref. 14.

Next, room temperature photoluminescence measurements were performed on the as-grown wafers to estimate the band gap of the $Ga_{1-x}In_xN_yAs_{1-y}$ layers in the wafers. The photoluminescence from the wafers due to excitation by 532 nm wavelength light was dispersed by a 0.5 m spectrometer and detected by a liquid nitrogen-cooled germanium detector. The wavelength at which the photoluminescence peaked was used to give the band gap of the $Ga_{1-x}In_xN_yAs_{1-y}$ layers. Due to the presence of the AlAs layer and the strong luminescence from the heavily doped GaAs layers on either side of the GaInNAs layer, significant cavity resonance peaks were seen in the photoluminescence spectra making it difficult to obtain any further information other than the peak position.

In both the x-ray rocking curve and photoluminescence measurements, the splitting between the $Ga_{1-x}In_xN_yAs_{1-y}$ layer and the GaAs substrate peaks as well as the photoluminescence peak wavelength were found to vary radially across the wafers. These variations translate into variation in nitrogen content and hence band gap of the $Ga_{1-x}In_xN_yAs_{1-y}$ layer across a single wafer. The nonuniformity across the wafers (with highest nitrogen content at the centers of the wafers) is attributed to the positioning of the nitrogen plasma source used in our growth system.

Figure 2 shows how the band gap (deduced from peak photoluminescence wavelengths) and x-ray peak splitting value vary across wafers B and C. It can be observed from Fig. 2 that the peak splitting changes from positive values toward the wafer center, which correspond to the $Ga_{1-x}In_xN_yAs_{1-y}$ layer being in tensile strain, to negative values toward wafer edge, which correspond to the $Ga_{1-x}In_xN_yAs_{1-y}$ layer being in compressive strain.

Moving from the wafer edge to the wafer center, the change in sign and magnitude of the peak splitting values, as shown on the right-hand axis, corresponds to an increasing nitrogen content and hence decreasing band gap in the $Ga_{1-x}In_xN_yAs_{1-y}$ layers, as shown on the left-hand axis. Assuming that the change in lattice mismatch seen in Fig. 2 is due to the variation in nitrogen content alone, it is estimated to vary from 3.8% to 2.6% as we move from the center to edge across wafer C. Nevertheless, the absolute range of peak splitting in the x-ray rocking curves across the wafers is relatively small and hence the $Ga_{1-x}In_xN_yAs_{1-y}$ layers used in this work are considered nominally lattice-matched to GaAs.

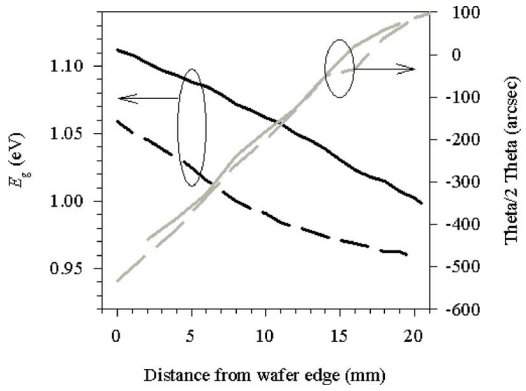

FIG. 2. Variations of band gap (left-hand axis) and x-ray peak splitting (right-hand axis) of the $Ga_{1-x}In_xN_yAs_{1-y}$ layers in wafers B (solid lines) and C (dashed lines) with position on wafers at room temperature.

IV. ELECTRICAL CHARACTERIZATION

The regions of the three wafers, on which x-ray data were described earlier, were then fabricated into devices for subsequent characterization. The estimated nitrogen contents and band gaps for the $Ga_{1-x}In_xN_yAs_{1-y}$ layers in the three wafers are as given in Table II.

To assess the unintentional doping concentration in the $Ga_{1-x}In_xN_yAs_{1-y}$ layers, capacitance-voltage characteristics were measured on these devices using a HP4275 LCR meter. The measured capacitance-voltage characteristics of different-sized devices scaled with device area. In addition, no significant frequency dependence was observed over a measurement frequency range from 10 kHz to 4 MHz, indicating that the measured capacitance was not affected by carrier trapping in the depleted regions. Doping concentrations in the unintentional doped $Ga_{1-x}In_xN_yAs_{1-y}$ layers were estimated from the measured capacitance-voltage characteristics, using Poisson's equation and assuming simple one-sided depletion.

Due to the undesirable effects of Debye blurring on the doping concentration profile, capacitance-voltage measurements were repeated at 77 K and the estimated doping concentration profiles for the three wafers are shown in Fig. 3. Devices were slightly forward-biased up to ~1 V so that complete doping concentration profiles for the unintentional doped $Ga_{1-x}In_xN_yAs_{1-y}$ layers were obtained. It can be seen from Fig. 3 that the unintentional doping concentrations drop rapidly to ~10^{14}–$10^{15}$$cm^{-3}$ away from the highly doped cladding layers. Such a low unintentional doping concentration enables full depletion of the 0.4 μm thick $Ga_{1-x}In_xN_yAs_{1-y}$ layers with only the built-in electric field. Hence, zero external voltage operation is possible for photodiodes made with narrow band gap $Ga_{1-x}In_xN_yAs_{1-y}$ layers. This is also an attractive attribute for solar cells. The correlation between ni-

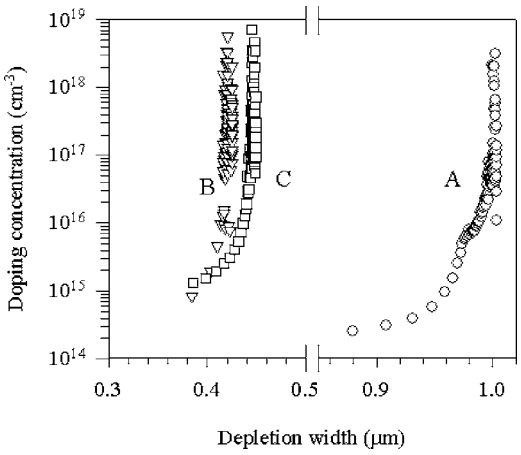

FIG. 3. Doping profiles estimated from capacitance-voltage characteristics of the wafers measured at 77 K.

trogen content and unintentional doping concentration in $Ga_{1-x}In_xN_yAs_{1-y}$ layers reported in Ref. 9 can also be observed from Fig. 3.

Room temperature dark current-voltage characteristics were measured on different-sized devices from the same three pieces. Both forward and reverse dark currents scaled with the device areas for all wafers, except for reverse current-voltage characteristics of wafer A, because the device dark currents of wafer A were below the lower measurement limit of the setup. The forward current-voltage characteristics showed an ideality factor of approximately 1.5 at low forward voltages for all wafers, indicating that both diffusion and recombination currents are significant.

The reverse current densities versus electric field of the three wafers are compared in Fig. 4. The electric field was estimated by assuming an ideal $p-i-n$ diode structure, the nominal $i-Ga_{1-x}In_xN_yAs_{1-y}$ layer thickness and a built-in voltage of 1 V. The sudden increase in current density for wafer A at 340 kV/cm is due to avalanche breakdown. The lower breakdown field for wafer A than wafers B and C is expected due to its much thicker i region. The lowest reverse current density data reported by Ref. 5, which were measured on a $Ga_{1-x}In_xN_yAs_{1-y}Sb$ $p-i-n$ diode wafer with a band gap and an i region thickness very similar to those of wafer C, are also plotted in Fig. 4 for comparison.

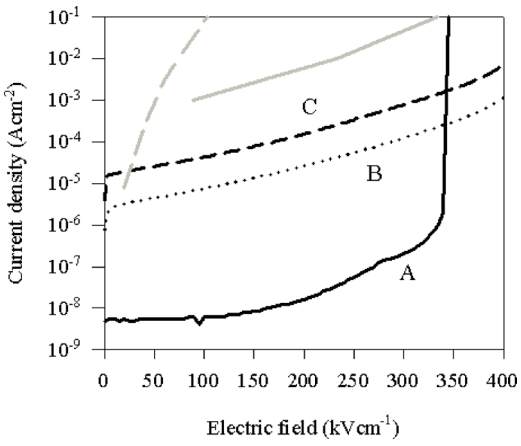

FIG. 4. Reverse current densities vs electric field of the wafers A, B, and C measured at room temperature (black lines). The data of a $Ga_{1-x}In_xN_yAs_{1-y}Sb$ diode (Ref. 5) (solid gray line) and a $Ga_{1-x}In_xN_yAs_{1-y}$ diode (Ref. 7) (dashed gray line), with i region thickness and band gap similar to those of wafer C, are also plotted for comparison.

It is clear from Fig. 4 that the reverse current characteristics of wafer C is significantly lower than the lowest reported in the literature.[5] Recent data of a $Ga_{1-x}In_xN_yAs_{1-y}$ $p-i-n$ diode,[7] again very similar to wafer C in terms of band gap and i region thickness, are significantly higher than the data of this work, as shown in Fig. 4. The significantly lower reverse leakage currents in our samples are attributed to better lattice matching to GaAs of our quaternary $Ga_{1-x}In_xN_yAs_{1-y}$ layers compared to those in Refs. 5 and 7.

It can be observed from Fig. 4 that our reverse current-voltage characteristics increase rapidly with nitrogen content in the $Ga_{1-x}In_xN_yAs_{1-y}$ layer. The shape of the reverse current-voltage characteristic is also unusual. For a $p-i-n$ diode, the two main mechanisms for bulk reverse leakage currents, namely diffusion and generation, generally do not increase significantly with reverse voltage. Note that the reverse electric fields shown in Fig. 4 are too low for band-to-band tunneling to be significant. If the observed trend in dark current continued, a further significant increase in nitrogen content could result in unacceptably large reverse currents for photodiodes.

The unusual increase in reverse dark current density with electric field observed in Fig. 4 may be caused by defects in the $Ga_{1-x}In_xN_yAs_{1-y}$ layers, which may exist as trapping levels in the forbidden gap. The defect density may increase with the nitrogen content, leading to higher trap-assisted tunneling current density. The difference in $Ga_{1-x}In_xN_yAs_{1-y}$ band gaps in wafers B and C may not be large enough to cause difference in slope of reverse dark current increase with electric field.

V. ELECTROLUMINESCENCE AND PHOTOCURRENT

Room temperature electroluminescence from the devices described earlier was also measured to confirm the values of the $Ga_{1-x}In_xN_yAs_{1-y}$ band gap deduced from photoluminescence data. The surface normal electroluminescence from forward-biased devices was collected and detected using the same setup used for photoluminescence measurements.

The data for wafers A, B, and C, obtained under an identical forward current density of 64 A/cm^2, are shown in Fig. 5. Electroluminescence peak wavelengths are 970 nm (1.28 eV), 1196 nm (1.04 eV), and 1276 nm (0.97 eV), with full width at half maxima (FWHM) values of 37, 51, and 51 meV, for wafers A, B, and C, respectively. The data of electroluminescence and photoluminescence gave consistent values of peak wavelength for the three wafers, confirming the accuracy of the band gap values used in this work.

We obtained further electroluminescence data from a GaAs $p-i-n$ diode at room temperature using the same experimental setup. FWHM of 44 meV was measured at room temperature, which is in good agreement with the lower limit due to thermal distribution of carrier energy (45 meV).[18] While wafers B and C have electroluminescence FWHM values close to that of GaAs $p-i-n$ diode, wafer A exhibits a

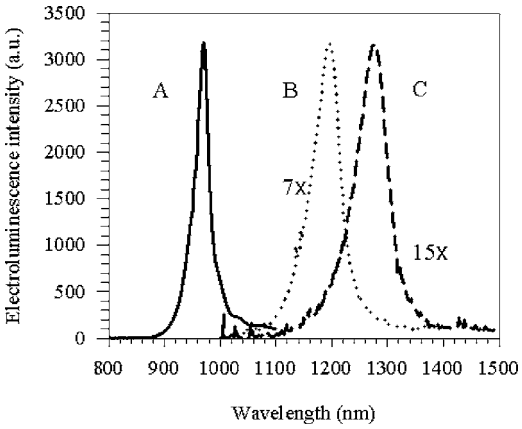

FIG. 5. Room temperature electroluminescence vs wavelength of wafers A, B, and C.

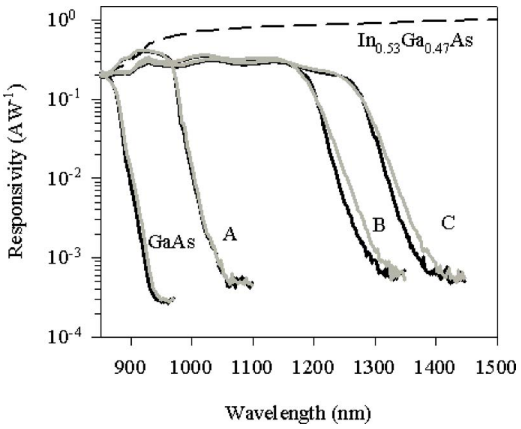

FIG. 6. Room temperature responsivity curves of wafers A, B, and C at 0 and −2 V. Specified and measured responsivity data for a commercial $In_{0.53}Ga_{0.47}As$ photodiode and an in-house GaAs 0.5 μm $p-i-n$ diode, respectively, are also shown for comparison.

smaller FWHM. This may be due to additional reflections at wavelengths coinciding with one of the optical cavity modes (discussed later) in wafer A.

However, increasing nitrogen content in the $Ga_{1-x}In_xN_yAs_{1-y}$ layer leads to a significant reduction of electroluminescence intensity, as shown in Fig. 5, indicating degradation of the optical quality of the devices. The optical and electrical (as observed in increased reverse dark current) degradation with increasing nitrogen content used in the wafers suggests the presence of nitrogen-related growth defects.

The usefulness of a wafer for photodiode applications is usually characterized by its responsivity, given by the ratio of photocurrent to incident optical power, versus wavelength. Hence, photocurrent measurements as function of wavelength were carried out on our devices. Note that the photocurrent and electroluminescence measurements were performed on the same devices for all three wafers to ensure consistency.

Spectrally dispersed light from a tungsten bulb and a monochromator was shone onto the device optical window (again using the same three pieces for wafers A, B, and C). A phase-sensitive detection technique was used to measure the photocurrent in the presence of dark currents. The incident optical power was measured using an EG&G C30665 $In_{0.53}Ga_{0.47}As$ photodiode. Responsivity curves as a function of wavelength for wafers A, B, and C at reverse voltages of 0 and 2 V are compared in Fig. 6, together with that of the C30665 photodiode for reference. Responsivity measurements were also carried out for an in-house GaAs homojunction $p-i-n$ diode with 0.5 μm thick i region grown on n^+ GaAs substrate. The data obtained for reverse voltages of 0 and 2 V are also shown in Fig. 6.

For our wafers, the values of the absorption band edge given by the responsivity curves agree with data of electroluminescence and photoluminescence. Significantly, the responsivity curves of a given wafer for the two reverse voltages used are very similar. This is expected from the low, unintentional doping concentration in the $Ga_{1-x}In_xN_yAs_{1-y}$ layer because it is already fully depleted at zero external voltage.

At a reverse voltage of 2 V, wafers A, B, and C have responsivities of 0.24 (1.28 eV), 0.13 (1.04 eV), and 0.11 (0.97 eV) A/W, respectively. These values compare well with the reported values of 0.097 A/W (Ref. 5) and 0.016A/W (Ref. 7) at 0.95 eV. Optical absorption up to a photon wavelength of ~1.38 μm was detected in wafer C, an as-grown antimony-free $Ga_{1-x}In_xN_yAs_{1-y}$ $p-i-n$ diode structure. The responsivity should be improved by employing antireflection coatings and increasing the i region thickness. Assuming the nominal total $Ga_{1-x}In_xN_yAs_{1-y}$ layer thicknesses (including the p- and n-doped $Ga_{1-x}In_xN_yAs_{1-y}$ cladding layers), optical power reflection loss of 32% from air to semiconductor and no other internal mechanisms for loss of carrier, absorption coefficients are calculated to be in the region of 4×10^3 (at 1.28 eV), 5×10^3 (at 1.04 eV), and 3×10^3 (at 0.97 eV) cm^{-1}, for wafers A, B, and C, respectively. These roughly obtained values are within an order of magnitude below those of $In_{0.53}Ga_{0.47}As$ for the same photon energies.[19]

Fringes can be observed in the responsivity spectra shown in Fig. 6 and they are attributed to the optical cavity formed between the air and the 100 nm AlAs layer. Assuming that $Ga_{1-x}In_xN_yAs_{1-y}$ has the same refractive index as that of GaAs (3.6), the spacing between the fringes yields cavity length values of 3500, 1425, and 1420 nm, for wafers A, B, and C, respectively. These values are close to the nominal values of semiconductor layer thickness above the AlAs layer in wafers A (3400 nm), B (1300 nm), and C (1300 nm).

VI. CONCLUSIONS

We have demonstrated high quality $Ga_{1-x}In_xN_yAs_{1-y}$ $p-i-n$ diodes lattice matched to GaAs with low unintentional doping concentration of ~10^{14} cm^{-3}, low reverse currents and an absorption edge down to 0.97 eV in a device with a responsivity of 0.11 A/W. This combination of desirable attributes was achieved without postgrowth annealing or addition of antimony.

ACKNOWLEDGMENT

The authors would like to thank the Engineering and Physical Sciences Research Council (EPSRC) for funding the work.

[1]M. Kondow, K. Uomi, A. Niwa, T. Kitatani, S. Watahiki, and Y. Yazawa, Jpn. J. Appl. Phys., Part 1 **35**, 1273 (1996).
[2]I. Tångring, S. M. Wang, M. Sadeghi, Q. F. Gu, and A. Larsson, J. Cryst. Growth **281**, 220 (2005).
[3]G. S. Kinsey, D. W. Gotthold, A. L. Holmes, B. G. Streetman, and J. C. Campbell, Appl. Phys. Lett. **76**, 2824 (2000).
[4]J. B. Héroux, X. Yang, and W. I. Wang, Appl. Phys. Lett. **75**, 2716 (1999).
[5]W. K. Cheah, W. J. Fan, S. F. Yoon, D. H. Zhang, B. K. Ng, W. K. Loke, R. Liu, and A. T. S. Wee,IEEE Photonics Technol. Lett. **17**, 1932 (2005).
[6]D. Jackrel, H. Yuen, S. Bank, M. Wistey, J. Fu, X. Yu, Z. Rao, and J. S. Harris, Proc. SPIE **5726**, 27 (2005).
[7]W. K. Loke, S. F. Yoon, S. Wicaksono, and B. K. Ng, Mater. Sci. Eng., B **131**, 40 (2006).
[8]A. R. Adams, IEEE Electron Device Lett. **40**, 1086 (2004).
[9]A. J. Ptak, D. J. Friedman, S. Kurtz, and R. C. Reedy, J. Appl. Phys. **98**, 094501 (2005).
[10]S. Kurtz, S. Johnston, and H. M. Branz, Appl. Phys. Lett. **86**, 113506 (2005).
[11]Z. Pan, L. H. Li, W. Zhang, Y. W. Lin, and R. H. Wu, Appl. Phys. Lett. **77**, 214 (2000).
[12]V. A. Odnoblyudov, A. Y. Egorov, A. R. Kovsh, A. E. Zhukov, N. A. Maleev, E. S. Semenova, and V. M. Ustinov, Semicond. Sci. Technol. **16**, 831 (2001).
[13]E. M. Pavelescu, J. Wagner, H. P. Komsa, T. T. Rantala, M. Dumitrescu, and M. Pessa, J. Appl. Phys. **98**, 083524 (2005).
[14]C. H. Fischer and P. Bhattacharya, J. Appl. Phys. **96**, 4176 (2004).
[15]S. Shirakata, M. Kondwo, and T. Kitatani, J. Phys. Chem. Solids **64**, 1533 (2003).
[16]D. J. Dunstan, P. Kidd, L. K. Howard, and R. H. Dixon, Appl. Phys. Lett. **59**, 3390 (1991).
[17]B. K. Tanner, A. G. Tnrnbull, C. R. Stanley, A. H. Kean, and M. McElhinney, Appl. Phys. Lett. **59**, 2272 (1991).
[18]E. O. Gobel, in *GaInAsP Alloy Semiconductor*, edited by T. P. Pearsall (Wiley, New York, 1982), Chap. 13, p. 319.
[19]S. Adachi, *Physical Properties of III-V Semiconductor Compounds* (Wiley, New York, 1992).